
This manuscript has been submitted for publication in *Geophysical Research Letters*. Please note that, the manuscript is currently under review and has yet to be formally accepted for publication. Subsequent versions of this manuscript may have slightly different content. If accepted, the final version of this manuscript will be available via the 'Peer-reviewed Publication DOI' link on the right-hand side of this webpage.

On the modulation of kinetic energy transfer by internal gravity waves

Adekunle Ajayi, UGA (adeajayi.kunle@gmail.com)

Julien Le Sommer, CNRS (julien.Lesommer@univ-grenoble-alpes.fr)

Laurent Brodeau, Datlas (lb.ocnxt@gmail.com)

Brian K. Arbic, U. Michigan (arbic@umich.edu)

Guillaume Sérazin, CNRS (guillaume.serazin@univ-brest.fr)

Aurélie Albert, CNRS (aurelie.albert@univ-grenoble-alpes.fr)

Takaya Uchida, CNRS (takaya.uchida@univ-grenoble-alpes.fr)

Patrice Klein, Caltech (pklein@caltech.edu)

On the modulation of kinetic energy transfer by internal gravity waves

Adekunle Ajayi¹, Julien Le Sommer¹, Laurent Brodeau^{2,3}, Brian K. Arbic⁴,
Guillaume Sérazin^{5,6}, Aurélie Albert¹, Takaya Uchida¹ and Patrice Klein^{7,8}

¹Université Grenoble Alpes/CNRS/IRD/IGE, Grenoble, France

²Ocean Next, Grenoble, France

³Datlas, Grenoble, France

⁴Department of Earth and Environmental Sciences, University of Michigan, Ann Arbor, MI, USA

⁵Climate Change Research Center, UNSW, Australia

⁶Université de Bretagne Occidentale/CNRS/Ifremer/IRD/LOPS, Plouzané, France

⁷Division of Geological and Planetary Sciences, California Institute of Technology, Pasadena, CA 91106,
USA

⁸LMD, Ecole Normale Supérieure/CNRS/IPSL, Paris, France

Key Points:

- Twin submesoscale-permitting simulations of the North Atlantic Ocean were run with and without tidal forcing.
- The tidally-forced run shows enhanced internal gravity wave (IGW) signal during summer while the non-tidally forced run during winter.
- Tidally-forced IGWs (i.e. internal tides) enhance forward cascade of kinetic energy particularly during summertime.

Corresponding author: Takaya Uchida, takaya.uchida@univ-grenoble-alpes.fr

21 **Abstract**

22 Understanding how kinetic energy (KE) is exchanged across scales and eventually dissipated
 23 remains a key question in physical oceanography. Recent theoretical works suggests that
 24 both quasi-balanced submesoscale motions and internal gravity waves (IGWs) could play
 25 a role in fluxing KE towards dissipation. How these classes of motions actually provide a
 26 route to dissipation in the ocean is still debated. This study investigates the impact of IGWs
 27 generated by tidal motions on cross-scale KE exchanges at mid-latitude. Our analysis is
 28 based on the output of two realistic submesoscale permitting ocean model simulations of the
 29 North Atlantic Ocean, run respectively with and without tidal forcing. These twin experi-
 30 ments permit investigation of how tidally-forced IGWs modify the KE variance, cross-scale
 31 exchanges, and associated seasonality. Our results show that, in the presence of externally-
 32 forced IGWs, KE transfer towards dissipative scales is enhanced in summertime both at the
 33 surface and in the ocean interior.

34 **Plain Language Summary**

35 Energetic oceanic currents on the scales of tens of kilometers that emerge as a re-
 36 sult of the chaotic nature of the ocean, known as (sub)mesoscale flows, have been of great
 37 scientific interest to the oceanographic community. These currents are associated with
 38 the time scales of roughly a day, which overlap with the astronomical tidal frequency of
 39 the ocean. Due to their similar time scales, it has been argued that the (sub)mesoscale
 40 flows and tides would interact with each other. Here, by running a twin numerical sim-
 41 ulation of the North Atlantic Ocean, one with tides and the other without, we examine
 42 the physical interaction between the two and show that the tides stimulate a loss of en-
 43 ergy from the (sub)mesoscale flows particularly during the summer.

44 **1 Introduction**

45 The ocean's kinetic energy is mostly concentrated in motions close to geostrophic balance,
 46 with frequencies lower than the Coriolis frequency (f) and spatial scales larger than the first
 47 Rossby deformation radius (R_d ; Vallis, 2017). These balanced motions (BMs) are largely
 48 energized through baroclinic instability which extracts energy from large scale stratification.
 49 Balanced motions include large-scale motions (> 300 km), mesoscale motions (50–300 km)
 50 and submesoscale balanced motions (< 50 km) (McWilliams, 2016). Balanced motions are
 51 characterized by an inverse cascade of energy (Scott & Wang, 2005; Scott & Arbic, 2007;
 52 Eden, 2007; Aluie et al., 2017), so they do not provide a route to dissipation by themselves.
 53 Therefore, energy has to be transferred from balanced motions to high-frequency unbalanced

54 motion for dissipation to occur. To equilibrate the well-known inverse cascade of energy, the
 55 ocean requires ageostrophic processes to extract energy from balanced motions. Documented
 56 mechanisms that might trigger a forward transfer of energy from balanced motions down
 57 to dissipate scale include for instance (but are not limited to) (i) bottom boundary-layer
 58 turbulence (Wunsch & Ferrari, 2004; Sen et al., 2008; Arbic et al., 2009), (ii) generation
 59 of lee waves by mesoscale eddies interacting with topography (Nikurashin & Ferrari, 2010;
 60 Nikurashin et al., 2013; Trossman et al., 2013, 2016), (iii) generation of internal waves by
 61 upper-ocean frontal instabilities (Danioux et al., 2012; Shakespeare & Taylor, 2014) and
 62 (iv) direct cascade of energy by energetic submesoscale motions (Capet et al., 2008; Ferrari
 63 & Wunsch, 2009; Molemaker et al., 2010; McWilliams, 2016). Overall, these studies have
 64 shown that, at fine-scale, there are two classes of motions that can provide efficient transfer
 65 of energy to dissipative scales; submesoscale motions and internal gravity waves.

66 Submesoscale motions are flow structures in the form of density fronts, filaments and to-
 67 pographic wakes at the surface and throughout the interior at scale smaller than $O(100\text{ km})$
 68 (McWilliams, 2016). Internal gravity waves (IGWs) are a particular class of fast propagating
 69 unbalanced motions with frequencies equal to or higher than the Coriolis frequency f and
 70 spatial scale ranging from $O(10\text{ m})$ to $O(100\text{ km})$. IGWs include wind-induced near-inertial
 71 waves with frequency near the Coriolis frequency and internal tides generated by large scale
 72 barotropic tidal flow over topographic features. Near-inertial waves are usually stronger in
 73 winter than in summer because they are driven by surface winds (D’Asaro, 1985) while the
 74 signature of internal tides (namely IGWs at tidal frequencies) in ocean fields is typically
 75 stronger in summer time (Gerkema et al., 2004). Recent works have highlighted that these
 76 two classes of motions—submesoscale motions and IGWs—are out of phase seasonally (Rocha
 77 et al., 2016). Submesoscale motions tend to be stronger than IGWs in wintertime. The
 78 emergence of submesoscales is due to winter favored mechanisms such as mixed layer in-
 79 stability, wind-induced frontal instability among other processes (Qiu et al., 2014; Sasaki
 80 et al., 2014; Callies, Flierl, et al., 2015; Brannigan et al., 2015; McWilliams, 2016; Uchida
 81 et al., 2019; Khatri et al., 2021). On the other hand, the kinetic energy associated with
 82 IGWs shows stronger amplitude in summertime. This is due to the intensification of vertical
 83 normal modes and shallow mixed layer (Callies, Ferrari, et al., 2015; Rocha et al., 2016).

84 A forward cascade is seen in spectral kinetic energy fluxes computed from gridded
 85 satellite altimeter products (Scott & Wang, 2005) at scales smaller than $O(100\text{ km})$. Later
 86 work (Arbic et al., 2013) argued that this forward cascade could be physically based, and
 87 related to energy transfer between mesoscale eddies and IGWs, but could also be due to
 88 the spatial and temporal smoothing inherent in the construction of present-day gridded
 89 altimeter products. In this study, we partly focus on the energy transfers involving IGWs.

90 Indeed, due to high-frequency winds and tidal motions, energy extraction via IGWs seems
 91 to be a highly probable mechanism of kinetic energy sinks for balanced motions (J. Thomas
 92 & Daniel, 2021). From a theoretical standpoint, there are so far essentially two well known
 93 and documented energy transfer mechanisms from balanced motions to IGWs away from
 94 topography, namely the *stimulated generation* of a forward cascade of kinetic energy by near-
 95 inertial waves from balanced flows (Gertz & Straub, 2009; Rocha et al., 2018; Barkan et
 96 al., 2021) and the *spontaneous generation* of near-inertial waves from balanced flows (Nagai
 97 et al., 2015; Shakespeare & Hogg, 2017). In stimulated generation, near-inertial waves are
 98 first introduced by external forcing (e.g. wind) at the inertial frequency and then grow
 99 by extracting energy from the balanced flow (Gertz & Straub, 2009; Barkan et al., 2017;
 100 L. N. Thomas, 2017) while spontaneous generation is the emission of waves by unbalanced,
 101 large Rossby number flow at density fronts without external forcing. These waves then
 102 radiate vertically downwards into the interior and amplify by extracting energy from deep
 103 balanced flow (Shakespeare & Hogg, 2017). Spontaneous generation is localized at sharp
 104 submesoscale fronts and is not very efficient at small Rossby numbers (Danioux et al., 2012;
 105 Nagai et al., 2015; Shakespeare & Hogg, 2017). On the other hand, stimulated generation
 106 is efficient at small Rossby numbers provided that the waves are forced externally.

107 As listed above, several studies have focused on the impact of wind-generated near-
 108 inertial waves on energy dissipation (e.g. Barkan et al., 2017; J. Thomas & Arun, 2020).
 109 In contrast, little is known as to the role of internal tides on kinetic energy exchanges
 110 (cf. Barkan et al., 2021). We know that internal tides contribute to the building up of
 111 internal gravity waves continuum (Garret-Munk spectra) and that their energy eventually
 112 contributes to diapycnal mixing in the ocean interior (Arbic et al., 2018). Whether internal
 113 tides could play a significant role in the down-scale transfer of mesoscale eddy kinetic en-
 114 ergy is yet to be fully explored. In this context, we here focus on investigating the role of
 115 IGWs (and particularly internal tides) on cross-scale kinetic energy exchanges in a regime
 116 with active submesoscale motions. Our results show that externally forced IGWs enhance
 117 KE dissipation in summertime by catalyzing energy transfer from balanced motion to dis-
 118 sipative scale. We do this by using a twin submesoscale resolving numerical simulations
 119 (with/without tides) of the North Atlantic Ocean with a horizontal resolution of $1/60^\circ$.
 120 The only difference between the two simulations is the inclusion of tidal forcing. This per-
 121 mits us to investigate how IGWs affect kinetic energy exchanges in the presence of active
 122 submesoscales motions.

123 This paper is organized as follows: in the next section, we describe the numerical
 124 simulations. Section 3 presents the seasonality of balanced motions and IGWs characterized
 125 by the kinetic energy frequency-wavenumber spectral density. The contribution of balanced

126 motions and IGWs to the kinetic energy transfer is presented in section 4. We discuss the
 127 impacts of this observed seasonality on the kinetic energy spectral flux in section 5, and we
 128 identify two different mechanisms that support a direct cascade of energy in a dynamical
 129 regime with/without tidal motions.

130 **2 North Atlantic Ocean Simulation**

131 In this study, we use numerical outputs from a NEMO-based submesoscale eddy-permitting
 132 simulations of the North Atlantic with a horizontal resolution of $1/60^\circ$ (eNATL60; Brodeau
 133 et al., 2020). eNATL60 is a spatially-extended version of NATL60 (Ajayi et al., 2020, 2021).
 134 The simulation spans the North Atlantic ocean from about 6°N up to the polar circle. In
 135 particular, this simulation has a horizontal grid spacing ranging from 1.6 km at 6°N to 0.9 km
 136 at 65°N . The model has 300 vertical levels with a resolution of 1 m at the top-most layers to
 137 better resolve a realistic surface boundary layer. In practice, the model effective resolution is
 138 about 10–15 km in wavelength, the same as the resolution of the anticipated Surface Water
 139 and Ocean Topography (SWOT) altimetry mission (Fu & Ubelmann, 2014). The initial
 140 and open boundary conditions are based on GLORYS2v3 ocean reanalysis with a relaxation
 141 zone at the northern boundary for sea-ice concentration and thickness. The atmospheric
 142 forcing is based on ERA-Interim (ECMWF; Dee et al., 2011), the grid and bathymetry follow
 143 (Ducousso et al., 2017). A third-order upwind advection scheme is used for both momentum
 144 and tracers in the model simulation to implicitly adapt lateral viscosity and diffusivity to
 145 flow properties. The model is spin-up for a period of 18 months, and a one-year simulation
 146 output from July 2009 to June 2010 is used in this study. eNATL60 has two identical runs (i)
 147 eNATL60 with tidal forcing herein referred to as eN60-WT and (ii) eNATL60 with no tidal
 148 forcing eN60-NT. The two simulations have perfectly the same configuration except for the
 149 inclusion of tidal motions in eN60-WT. In the rest of this article, we use eNATL60 to refer to
 150 the two simulations while individual runs are addressed as eN60-WT (with tides) or eN60-
 151 NT (no tides). The inclusion of tidal forcing in eN60-WT run provides conversion of tidal
 152 energy into the internal wave field through, both, flow-topography interactions and wave-
 153 balanced motions interactions (Arbic et al., 2008, 2018). Consequently, the comparison of
 154 resolved dynamics between the two simulations allows diagnosing the impacts of the internal
 155 tides on cross-scale energy transfer in the North Atlantic.

156 To investigate cross-scale energy exchanges between different scales of motions, we esti-
 157 mate kinetic energy spectral density in frequency-wavenumber space as a proxy to under-
 158 stand the energetic nature of balanced/unbalanced motions in regimes with/without tidal
 159 motions. Also, we estimate the rate at which nonlinear mechanisms exchange energy across
 160 temporal and spatial scales in the two scenarios. In what follows, our analysis of kinetic

161 energy density and transfer is based on the hourly output of horizontal total velocity field
 162 and are computed using the following equation;

$$\frac{\partial \widehat{KE}}{\partial t} = T_{KE} + \widehat{\mathbf{u}}^* \cdot OT \quad (1)$$

$$\widehat{KE} = \frac{1}{2} \widehat{\mathbf{u}}^* \cdot \widehat{\mathbf{u}} \quad (2)$$

$$T_{KE} = -\widehat{\mathbf{u}}^* \cdot [\mathbf{u} \cdot \widehat{\nabla} \mathbf{u}] \quad (3)$$

163 Equations (1)–(3) are derived from the Fourier transform of momentum equation mul-
 164 tiplied by horizontal velocity field (Scott & Wang, 2005; Capet et al., 2008; Müller et al.,
 165 2015). In the momentum equation (Equation 1), KE and T_{KE} represents the kinetic energy
 166 density and kinetic energy transfer respectively while OT stands “Other Terms”. $\widehat{[]}$ refers
 167 to Fourier transform and $*$ represents the complex conjugate. Before performing spectral
 168 analysis the 2D time series were de-trended and windowed in space and time. The procedure
 169 performed in this study is consistent with standard procedures previously used in Rocha et
 170 al. (2016), Müller et al. (2015) and Torres et al. (2018).

171 The eNATL60 simulation resolves well to a reasonable extent, mesoscale motions, sub-
 172 mesoscale motions, and IGWs (see Figure 1 in SI). The comparison of eNATL60 sea surface
 173 height (SSH) spectral density with SARAL AltiKa (Figure 1a) shows that the predicted
 174 SSH variance by the model compares well with the satellite observation for scales > 100 km.
 175 There are differences at scales < 100 km that are due to the satellite instrument noise level.
 176 There seems to be quite a robust agreement between the two runs of eNATL60 simulations in
 177 wintertime. However, of particular interest is the difference between the runs in summertime
 178 where variance at fine-scales is of higher magnitude in eN60-WT than to eN60-NT.

179 A similar analysis of the kinetic energy spectral density in the same region (Figure 1b),
 180 shows that the variance associated with fine-scale motions smaller than 100 km is higher in
 181 the eN60-WT compared to eN60-NT. So what are the mechanism/dynamics at fine-scales
 182 in eN60-WT that could be responsible for this higher variance? A possible answer to this is
 183 that the inclusion of tidal motion in eN60-WT simulation is responsible for enhanced wave
 184 activity, and this is why we see higher variance at fine scales in the SSH and KE spectra
 185 density plot. To qualitatively investigate this, we separate the flow into its rotational and
 186 divergent part, which represents the balanced and the unbalanced wave motions, respec-
 187 tively. Figure 1c presents the spectral density for these two components. The spectra of

188 the rotational part for the two runs are almost indistinguishable, indicating that both sim-
 189 ulations have nearly equal energy levels in geostrophically balanced motions. However, the
 190 divergence spectra of the kinetic energy is very different between the two simulations. This
 191 difference is obvious at scales less than 500 km, and indeed, the divergent motions are more
 192 energetic in eN60-WT by a factor of 2 with two interesting peaks. We can conclude that
 193 the higher variance in eN60-WT at fine-scales compared to eN60-NT is primarily due to
 194 stronger divergent motions in eN60-WT, which is caused by the inclusion of tidal forcing in
 195 this simulation.

196 **3 Seasonality of BMs and IGWs**

197 This section presents the different classes of motions and their seasonality based on
 198 frequency-wavenumber spectral density. This diagnostic will help us better understand how
 199 the difference in wave activity between the two simulations affects oceanic motions' spectral
 200 signature across different temporal and spatial scales. For simplicity, we refer to frequency-
 201 horizontal wavenumber spectra as ω - K spectra. Following Torres et al. (2018), we begin by
 202 presenting a schematic (Figure 2a) showing the different observable dynamical regimes in the
 203 ocean as a function of their temporal and spatial scale. These classes of motions starting with
 204 low-frequency, low-wavenumber motions to high-frequency, high-wavenumber motions are
 205 Rossby waves (RW), mesoscale balanced motions (MBM), submesoscale balanced motions
 206 (SBM), unbalanced submesoscale motions (USM) and internal gravity waves (IGW). In this
 207 study, we focus on understanding how IGWs and BMs (in the presence of tidal motions)
 208 affect cross-scale energy exchanges. Due to the computational cost of this diagnostic tool,
 209 we perform the ω - K spectra analysis in a $5^\circ \times 5^\circ$ (-40° to -35° , 40° to 45°) box located
 210 inside the previous large box (see Figure 1 of SI).

211 We also show, in Figure 2, the winter and summer averages of surface KE ω - K spectra
 212 for the two runs. In the figure, the upper panel corresponds to eN60-NT and the lower panel
 213 to eN60-WT. The classes of motions described previously in Figure 2a are identifiable in the
 214 figure. The winter-summer contrast shows a strong seasonality in the spectral density of
 215 submesoscale BMs and IGWs. In wintertime, for eN60-WT (simulation with tidal forcing),
 216 energy is mostly concentrated in BMs, near-inertial waves, and the dispersion curve of IGWs
 217 (Figure 2b), while in summertime, energy is mostly concentrated in the mesoscale BMs, near-
 218 inertial waves, and internal tides (Figure 2d). In particular, the variance associated with
 219 submesoscale BMs is stronger in winter, while that of IGWs is stronger in summer. Our
 220 understanding is that IGWs are stronger in summer due to shallow mixed layer depth and
 221 vertical normal modes' intensification. At the same time, submesoscale BMs are stronger in
 222 winter because they are driven by winter-favored mechanisms such as frontogenesis, wind-

223 induced frontal instabilities, and mixed layer instability, among other processes (Qiu et al.,
 224 2014; Sasaki et al., 2014; Callies, Flierl, et al., 2015; Brannigan et al., 2015; McWilliams,
 225 2016; Uchida et al., 2019; Khatri et al., 2021). This out of phase seasonality of submesoscale
 226 BMs and IGWs is consistent with the findings of Rocha et al. (2016) and Torres et al. (2018).

227 Similarly, eN60-NT (simulation without tidal forcing) resolves the same classes of mo-
 228 tion as eN60-WT except that internal tides are absent and supertidal IGWs are less energetic
 229 in this simulation. In wintertime, energy is mostly concentrated in BMs, near-inertial waves,
 230 and along the dispersion curve of IGWs (Figure 2a). This is consistent with the winter dy-
 231 namics in eN60-WT. In summertime, energy is concentrated in mesoscale balanced motions
 232 and near-inertial waves (Figure 2c). Unlike eN60-WT, the seasonality observed in eN60-NT
 233 is associated with stronger submesoscale BMs and IGWs in winter. The seasonality of IGWs
 234 is reversed in eN60-NT when compared to eN60-WT (simulation with tidal forcing). How
 235 can this be? We know that the classical paradigm for the generation of the supertidal IGW
 236 continuum is that winds produce near-inertial waves, barotropic tidal flow over topographic
 237 features creates internal tides, and the energy along the IGW dispersion curve is due to
 238 nonlinear interactions. Both simulations are forced with realistic high-frequency winds with
 239 3-hourly outputs (Brodeau et al., 2020). These winds are stronger in winter, hence there is
 240 a well-resolved near-inertial wave and IGWs dispersion curve in winter. The dynamics in
 241 summertime are different between the two runs. For the eN60-WT simulation, internal tides
 242 generated by tidal motions are amplified by a shallow mixed layer in summertime, and non-
 243 linearity produces energy in the IGW dispersion curve. Thus for eN60-NT, the mechanism
 244 for generating waves in summertime is relatively weak; no tidal forcing and weaker winds,
 245 hence relatively weak wave motions in summer. The difference in the spectral energy density
 246 of different dynamical regimes between the two simulations extends below the surface (see
 247 Figure 3 of SI).

248 To obtain frequency spectra, we integrate the ω - K spectra over all wavenumbers for the
 249 two runs (Figure 3). In summertime, the variance at high frequencies (M_2 and supertidal
 250 frequencies) is higher in eN60-WT compared to eN60-NT. We believe that this is likely
 251 due to the amplification of internal gravity waves by tidal motions. eN60-WT spectra
 252 approximately follow the estimated Garrett-Munk spectra (Garrett & Munk, 1975; Cairns
 253 & Williams, 1976; Müller et al., 2015) in summertime. Visible in eN60-WT spectra are the
 254 peaks at the inertia frequency f and the M_2 tidal frequency. In contrast, only the near-
 255 inertial peak is visible in eN60-NT. To a large extent, we now understand the dynamics
 256 responsible for the differences in kinetic energy density that we see in the two simulations.
 257 In the following sections, we shall discuss how the enhanced IGWs arising from tidal forcing
 258 affect the redistribution of energy in different dynamical regimes.

4 Modulation of KE forward flux by IGWs

In this section, we will discuss the impact of resolving internal tides on the magnitude and direction of KE cascade at fine-scales in the wavenumber and frequency-wavenumber domain by comparing the twin eNATL60 runs.

4.1 Wavenumber KE flux

We start by examining the KE flux in the wavenumber domain. We do this by estimating the net energy (spectral flux) passing through individual wavenumbers in spectral space. The spectral flux is obtained by integrating the energy transfer (Equation 3) from a particular wavenumber K to K_0 (the wavenumber corresponding to the box size).

We present in Figure 4a,d, the winter and summer averages of kinetic energy spectral flux for both simulations. In wintertime and in the two simulations (Figure 4a), the flux is nearly identical across all wavenumbers. The forward cascade starts at around 25 km and extends down to a kilometric scale. In summertime (Figure 4d), the magnitude of the forward cascade at high wavenumbers differs significantly between the two runs. The inclusion of tidal forcing in eN60-WT yields a forward flux at high wavenumbers that is a factor of 4 higher than the forward high-wavenumber flux in eN60-NT. This difference in cascade highlights how internal tides enhance the forward cascade of kinetic energy at high wavenumbers.

Thus far, the kinetic energy cascade has been estimated only at the surface. Considering we have three-dimensional information of the ocean, as opposed to satellite observations, it is of great interest to understand the nature of the kinetic energy cascade in the ocean's interior. In Figure 4b,c,e,f, we present the spectral flux computed at 32 different vertical levels in the upper 1000 m of the water column. In winter and summer, at lower wavenumbers, the average KE flux in the two simulations is characterized by a net inverse cascade that extends down to around 700 m in the interior. In wintertime, the forward cascade at higher wavenumbers in eN60-WT (Figure 4c) is strong both at the surface and in the interior. In contrast, in eN60-NT (Figure 4b), the forward cascade is confined mostly to the surface. In summertime, the forward cascade in eN60-WT (Figure 4f) span the upper ocean but with a gradual decrease in magnitude farther down the water column. In contrast, in eN60-NT (Figure 4e), the forward cascade is nearly absent throughout the upper ocean. A stronger forward cascade (in summertime for eN60-WT) in the interior is an indication that internal tides transfer substantial amounts of kinetic energy to dissipative scales throughout the upper ocean water column.

4.2 Frequency-wavenumber KE transfer

We have demonstrated that internal tides enhance the supertidal IGW continuum and, in particular, enhance the forward cascade of energy in summertime. To better explain how internal tides modify cross-scale energy exchanges among the different classes of motions, we present in Figure 5 the winter and summer averages of kinetic energy spectral transfer in frequency-wavenumber space. In the ω - K spectra, negative values of spectra transfer imply that non-linearity extracts energy from these regions to feed other regions with positive values. In other words, sinks of energy are characterized by positive values, while sources of energy have negative values.

We start by discussing the spectral transfer in wintertime (cf. Equation 3; Figures 5a,c). In eN60-NT, the spectral transfer's positive values (blue) show that balanced motions serve as a source of energy for other motions, namely energy is being extracted from the balanced motions. In contrast, near-inertial motions and motions with scales less than 10 km are the major sinks of kinetic energy (red). The rate of non-linear exchanges in eN60-WT is similar to eN60-NT except for the mild intensification of energy gained by IGWs in eN60-WT. To summarize, submesoscale motions and internal gravity waves are sinks of kinetic energy in wintertime, with the former playing the major role.

The summer spectra (Figure 5b,d) differ significantly between the two runs as expected. In eN60-NT, balanced motions represent the major source of energy for other motions, while energy is gained mostly by near-inertial motions. The transfer at high frequencies and wavenumbers is very small. We can interpret this to signify that high-frequency motions and submesoscale motions are less energetic in eN60-NT in summertime. This result is consistent with results in the KE spectra density. But in eN60-WT, the situation is different. The major energy source for other motions is the mesoscale balanced motions and the semi-diurnal tides (blue). Near-inertial waves, submesoscale BMs and the supertidal IGW continuum spectrum are seen in Figure 5 to be gaining energy. The extraction of semi-diurnal tidal energy, and gain of energy in the IGW continuum, due to nonlinear interactions was also seen in (Müller et al., 2015) but is more clear here, perhaps because of the finer vertical and horizontal grid spacing in eN60-WT.

In summary, there are two mechanisms of energy extraction in summertime. (i) In a flow without tidal forcing, near-inertial waves gain energy from balanced motions, and (ii) in a flow with tidal forcing, near-inertial waves and the supertidal IGW continuum gain energy from internal tides and mesoscale balanced motions. In summary, the forward cascade in eN60-WT, is associated with the transfer of energy by nonlinearity from balanced motions and internal tides to near-inertial waves and the supertidal IGW continuum. This transfer

327 is possible due to the intensification of IGWs in the presence of tidal motions. The lack of
328 tidal motions in eN60-NT (compared to eN60-WT) shows how effective internal tides are
329 in providing a route to energy dissipation in summertime, both at the surface and in the
330 interior. This result strongly emphasizes the need to include tidal forcing in ocean model
331 simulations to accurately predict cross-scale energy exchanges at fine-scales.

332 5 Summary and conclusion

333 The role of internal tides in the seasonality of kinetic energy density and spectral kinetic
334 energy transfer was investigated in this study. Our analysis was based on the output of a
335 realistic NEMO simulation of the North Atlantic Ocean with a horizontal resolution of
336 $1/60^\circ$. We used two outputs of this numerical experiment; one with, and one without,
337 tidal forcing. These twin experiments permit investigation of how internal gravity waves (in
338 particular internal tides) generated by tidal forcing modify kinetic energy variance, cross-
339 scale exchanges, and associated seasonality. We found that the seasonality of IGWs is
340 sensitive to tidal forcing. In the simulation without tides, IGWs are stronger in winter,
341 whereas, in simulation with tides, they are stronger in summer. The latter condition is
342 consistent with the findings of Rocha et al. (2016) and Torres et al. (2018).

343 Our results also show that resolving internal tides in the presence of energetic subme-
344 soscale motions has a strong impact on kinetic energy transfer in summertime (cf. Barkan
345 et al., 2021, their Figure 3d,f). The magnitude of the estimated forward cascade at high
346 wavenumbers (both at the surface and at depth) in the simulation with tidal forcing is a fac-
347 tor 4 higher than in the simulation without tidal forcing (Figure 4). Overall, we identified
348 that two mechanisms supporting the kinetic energy forward cascade; (i) forward cascade
349 due to energetic submesoscale motions in wintertime and (ii) forward cascade due to IGWs
350 (enhanced by tidal forcing) in summertime (Figure 5). Our results underscore that at fine-
351 scales, internal tides can provide an effective route to kinetic energy dissipation.

352 In light of the SWOT altimeter mission (Morrow et al., 2019; Torres et al., 2019), the
353 difference between the runs with tidal forcing and without (e.g. Figures 1 and 3) highlight
354 the importance of tidal forcing in emulating the upcoming altimeter observations (Arbic et
355 al., 2018; Barkan et al., 2021; Yu et al., 2021).

356

Data Availability Statement

The twin eNATL60 data are permanently stored at the CINES supercomputing center in Montpellier, France. The regional dataset used for this study is available upon request to AAl (aurelie.albert@univ-grenoble-alpes.fr).

Acknowledgments

AAj was partly funded by the Université Grenoble Alpes AGIR research grant. JLS, LB and AAl acknowledge the PRACE 16th call project ReSuMPTiOn (Revealing Sub-Mesoscale Processes and Turbulence in the Ocean, P.I.: LB) for awarding access to the MareNostrum supercomputer at the Barcelona Supercomputing Center. JLS acknowledges support from Centre National d'Etudes Spatiales (MIDAS project) and Agence Nationale pour la Recherche (ANR-17-CE01-0009-01). BKA acknowledges support from NASA grants NNX16AH79G, NNX17AH55G, and 80NSSC20K1135. BKA began collaborations with the Grenoble group while on sabbatical in France, and he thanks many French colleagues, especially Thierry Penduff, Rosemary Morrow, and Nadia Ayoub, for their help in procuring this sabbatical year. PK is supported by the NASA NPP Senior Fellowship and the SWOT and S-Mode projects. TU acknowledges support from the French 'Make Our Planet Great Again' (MOPGA) initiative managed by ANR under the Programme d'Investissement d'Avenir, with the reference ANR-18-MPGA-0002.

References

- 375
376 Ajayi, A., Le Sommer, J., Chassignet, E., Molines, J., Xu, X., Albert, A., & Cosme, E.
377 (2020). Spatial and Temporal Variability of the North Atlantic Eddy Field From
378 Two Kilometric-Resolution Ocean Models. *J. Geophys. Res. Ocean.*, *125*(5). doi:
379 10.1029/2019jc015827
- 380 Ajayi, A., Le Sommer, J., Chassignet, E., Molines, J., Xu, X., Albert, A., & Dewar, W.
381 (2021). Diagnosing crossscale kinetic energy exchanges from two submesoscale per-
382 mitting ocean models. *JAMES*. doi: 10.1029/2019MS001923
- 383 Aluie, H., Hecht, M., & Vallis, G. K. (2017). Mapping the Energy Cascade in the North
384 Atlantic Ocean: The Coarse-graining Approach. *J. Phys. Oceanogr.*, *225*–244. doi:
385 10.1175/JPO-D-17-0100.1
- 386 Arbic, B. K., Alford, M., Ansong, J., Buijsman, M., Ciotti, R., Farrar, J., ... Zhao, Z.
387 (2018). A primer on global internal tide and internal gravity wave continuum modeling
388 in HYCOM and MITgcm. In E. Chassignet, A. Pascual, J. Tintoré, & J. Verron (Eds.),
389 *New frontiers in operational oceanography* (pp. 307–392). GODAE Ocean View. doi:
390 10.17125/gov2018.ch13
- 391 Arbic, B. K., Mitrovica, J. X., MacAyeal, D. R., & Milne, G. A. (2008). On the fac-
392 tors behind large Labrador Sea tides during the last glacial cycle and the potential
393 implications for Heinrich events. *Paleoceanography*, *23*.
- 394 Arbic, B. K., Polzin, K. L., Scott, R. B., Richman, J. G., & Shriver, J. F. (2013). On eddy
395 viscosity, energy cascades, and the horizontal resolution of gridded satellite altimeter
396 products. *J. Phys. Oceanogr.*, *43*, 283–300. doi: 10.1175/JPO-D-11-0240.1
- 397 Arbic, B. K., Shriver, J. F., Hogan, P. J., Hurlburt, H. E., McClean, J. L., Metzger, E. J.,
398 ... Wallcraft, A. J. (2009). Estimates of Bottom Flows and Bottom Boundary Layer
399 Dissipation of the Oceanic General Circulation from Global High-Resolution Models.
400 *J. Geophys. Res.*, *114*, C02024. doi: 10.1029/2008JC005072
- 401 Barkan, R., Srinivasan, K., Yang, L., McWilliams, J. C., Gula, J., & Vic, C. (2021). Oceanic
402 mesoscale eddy depletion catalyzed by internal waves. *Geophysical Research Letters*,
403 *48*(18), e2021GL094376. doi: 10.1029/2021GL094376
- 404 Barkan, R., Winters, K. B., & McWilliams, J. C. (2017). Stimulated Imbalance and the En-
405 hancement of Eddy Kinetic Energy Dissipation by Internal Waves. *J. Phys. Oceanogr.*,
406 *47*(1), 181–198.
- 407 Brannigan, L., Marshall, D. P., Naveira-Garabato, A., & George Nurser, A. J. (2015).
408 The seasonal cycle of submesoscale flows. *Ocean Modelling*, *92*, 69–84. doi: 10.1016/
409 j.ocemod.2015.05.002
- 410 Brodeau, L., Albert, A., & Le Sommer, J. (2020). *NEMO-eNATL60 description and as-*
411 *essment repository*. doi: 10.5281/zenodo.4032732

- 412 Cairns, J., & Williams, G. (1976). Internal wave observations from a midwater float.
413 *JAMES*, 81(12), 1943–1950. doi: 10.1029/JC081i012p01943
- 414 Callies, J., Ferrari, R., Klymak, J. M., & Gula, J. (2015). Seasonality in submesoscale
415 turbulence. *Nature Communication*, 6, 6862.
- 416 Callies, J., Flierl, G., Ferrari, R., & Fox-Kemper, B. (2015). The role of mixed-layer
417 instabilities in submesoscale turbulence. *J. Fluid Mech.*, 788, 5–41.
- 418 Capet, X., Klein, P., Hua, B. L., Lapeyre, G., & McWilliams, J. C. (2008). Surface kinetic
419 energy transfer in surface quasi-geostrophic flows. *J. Fluid Mech.*, 604, 165–174.
- 420 Danioux, E., Vanneste, J., Klein, P., & Sasaki, H. (2012). Spontaneous inertia-gravity-
421 wave generation by surface-intensified turbulence. *Journal of Fluid Mechanics*, 699,
422 153173.
- 423 D’Asaro, E. A. (1985). The Energy Flux from the Wind to Near-Inertial Motions in the
424 Surface Mixed Layer. *J. Phys. Oceanogr.*, 15, 1043–1059.
- 425 Dee, D. P., Uppala, S. M., Simmons, A., Berrisford, P., Poli, P., Kobayashi, S., ... oth-
426 ers (2011). The era-interim reanalysis: Configuration and performance of the data
427 assimilation system. *Quarterly Journal of the royal meteorological society*, 137(656),
428 553–597. doi: 10.1002/qj.828
- 429 Ducouso, N., Le Sommer, J., Molines, J. M., & Bell, M. (2017). Impact of the symmet-
430 ric instability of the computational kind at mesoscale- and submesoscale-permitting
431 resolutions. *Ocean Modelling*, 120(18–26).
- 432 Eden, C. (2007). Eddy length scales in the North Atlantic Ocean. *Journal of Geophysical*
433 *Research*, 112(C6), C06004.
- 434 Ferrari, R., & Wunsch, C. (2009). Ocean Circulation Kinetic Energy: Reservoirs, Sources,
435 and Sinks. *Annu. Rev. Fluid Mech.*, 41(1), 253–282.
- 436 Fu, L. L., & Ubelmann, C. (2014). On the transition from profile altimeter to swath
437 altimeter for observing global ocean surface topography. *J. Atmos. Oceanic Technol.*,
438 31, 560–568.
- 439 Garrett, C., & Munk, W. (1975). Space-time scales of internal waves: A progress report.
440 *JAMES*, 80(3), 291–297. doi: 10.1029/JC080i003p00291
- 441 Gerkema, T., Lam, F.-P. A., & Maas, L. R. (2004). Internal tides in the Bay of Biscay:
442 conversion rates and seasonal effects. *Deep Sea Research Part II: Topical Studies in*
443 *Oceanography*, 51(25–26), 2995–3008. doi: 10.1016/j.dsr2.2004.09.012
- 444 Gertz, A., & Straub, D. N. (2009). Near-Inertial Oscillations and the Damping of Mid-
445 latitude Gyres: A Modeling Study. *J. Phys. Oceanogr.*, 39(9), 2338–2350. doi:
446 10.1175/2009jpo4058.1
- 447 Khatri, H., Griffies, S. M., Uchida, T., Wang, H., & Menemenlis, D. (2021). Role of mixed-
448 layer instabilities in the seasonal evolution of eddy kinetic energy spectra in a global

- 449 submesoscale permitting simulation. *Geophysical Research Letters*, e2021GL094777.
450 doi: 10.1029/2021GL094777
- 451 McWilliams, J. C. (2016). Submesoscale currents in the ocean. *Proc. R. Soc., A* 472,
452 20160117.
- 453 Molemaker, M. J., McWilliams, J. C., & Capet, X. (2010). Balanced and unbalanced routes
454 to dissipation in an equilibrated eady flow. *Journal of Fluid Mechanics*, 654, 35–63.
455 doi: 10.1017/S0022112009993272
- 456 Morrow, R., Fu, L.-L., Ardhuin, F., Benkiran, M., Chapron, B., Cosme, E., ... Zaron,
457 E. D. (2019). Global Observations of Fine-Scale Ocean Surface Topography With the
458 Surface Water and Ocean Topography (SWOT) Mission. *Frontiers in Marine Science*,
459 6. doi: 10.3389/fmars.2019.00232
- 460 Müller, M., Arbic, B. K., Richman, J. G., Shriver, J. F., Kunze, E. L., Scott, R. B., ...
461 Zamudio, L. (2015). Toward an internal gravity wave spectrum in global ocean models.
462 *Geophys. Res. Lett.*, 42, 34743481.
- 463 Nagai, T., Tandon, A., Kunze, E., & Mahadevan, A. (2015). Spontaneous Generation of
464 Near-Inertial Waves by the Kuroshio Front. *J. Phys. Oceanogr.*, 45(9), 2381–2406.
465 doi: 10.2139/ssrn.2906136
- 466 Nikurashin, M., & Ferrari, R. (2010). Radiation and Dissipation of Internal Waves Generated
467 by Geostrophic Motions Impinging on Small-Scale Topography: Theory. *J. Phys.*
468 *Oceanogr.*, 40(9), 2025–2042. doi: 10.1175/2010JPO4315.1
- 469 Nikurashin, M., Vallis, G. K., & Adcroft, A. (2013). Routes to energy dissipation for
470 geostrophic flows in the Southern Ocean. *Nat. Geosci.*, 6(1), 48–51. doi: 10.1038/
471 ngeo1657
- 472 Qiu, B., Chen, S., Klein, P., Sasaki, H., & Sasai, Y. (2014). Seasonal Mesoscale and
473 Submesoscale Eddy Variability along the North Pacific Subtropical Countercurrent.
474 *Journal of Physical Oceanography*, 44(12), 3079 - 3098.
- 475 Rocha, C. B., Gille, S. T., Chereskin, T. K., & M., D. (2016). Seasonality of submesoscale
476 dynamics in the Kuroshio Extension. *Geophysical Research Letters*, 43, 11304 - 11311.
- 477 Rocha, C. B., Wagner, G. L., & Young, W. R. (2018). Stimulated generation: Extraction
478 of energy from balanced flow by near-inertial waves. *J. Fluid Mech.*, 847, 417–451.
- 479 Sasaki, H., Klein, P., Qiu, B., & Sasai, Y. (2014). Impact of oceanic scale- interactions on the
480 seasonal modulation of ocean dynamics by the atmosphere. *Nature Communication*,
481 5, 5636.
- 482 Scott, R. B., & Arbic, B. K. (2007). Spectral Energy Fluxes in Geostrophic Turbulence:
483 Implications for Ocean Energetics. *J. Phys. Oceanogr.*, 37(3), 673–688. Retrieved
484 from <http://journals.ametsoc.org/doi/abs/10.1175/JP03027.1> doi: 10.1175/
485 JPO3027.1

- 486 Scott, R. B., & Wang, F. (2005). Direct Evidence of an Oceanic Inverse Kinetic Energy
487 Cascade from Satellite Altimetry. *J. Phys. Oceanogr.*, *35*, 1650–1666. Retrieved
488 from <http://journals.ametsoc.org/doi/abs/10.1175/JPO2771.1> doi: 10.1175/
489 JPO2771.1
- 490 Sen, A., Scott, R. B., & Arbic, B. K. (2008). Global Energy Dissipation Rate of Deep-
491 Ocean Low-Frequency Flows by Quadratic Bottom Boundary Layer Drag: Compu-
492 tations from Current Meter Data. *Geophys. Res. Lett.*, *35*, L09606. doi: 10.1029/
493 2008GL033407
- 494 Shakespeare, C. J., & Hogg, A. M. (2017). Spontaneous Surface Generation and Interior
495 Amplification of Internal Waves in a Regional-Scale Ocean Model. *J. Phys. Oceanogr.*,
496 *47*(4), 811–826.
- 497 Shakespeare, C. J., & Taylor, J. R. (2014). The spontaneous generation of inertia-gravity
498 waves during frontogenesis forced by large strain: Theory. *J. Fluid Mech.*, *757*, 817 -
499 853.
- 500 Thomas, J., & Arun, S. (2020). Near-inertial waves and geostrophic turbulence. *Physical*
501 *Review Fluids*, *5*(1), 014801. doi: 10.1103/PhysRevFluids.5.014801
- 502 Thomas, J., & Daniel, D. (2021). Forward flux and enhanced dissipation of geostrophic
503 balanced energy. *Journal of Fluid Mechanics*, *911*. doi: 10.1017/jfm.2020.1026
- 504 Thomas, L. N. (2017). On the modifications of near-inertial waves at fronts: implications
505 for energy transfer across scales. *Ocean Dyn.*, *67*(10), 1335–1350.
- 506 Torres, H. S., Klein, P., Menemenlis, D., Qiu, B., Su, Z., Wang, J., . . . Fu, L. L. (2018).
507 Partitioning Ocean Motions Into Balanced Motions and Internal Gravity Waves: A
508 Modeling Study in Anticipation of Future Space Missions. *J. Geophys. Res. Ocean.*,
509 *123*, 8084–8105. doi: 10.1029/2018JC014438
- 510 Torres, H. S., Klein, P., Siegelman, L., Qiu, B., Chen, S., Ubelmann, C., . . . Fu, L.-L.
511 (2019). Diagnosing ocean-wave-turbulence interactions from space. *Geophysical Re-*
512 *search Letters*, *46*(15), 8933–8942. doi: 10.1029/2019GL083675
- 513 Trossman, D. S., Arbic, B. K., Garner, S. T., Goff, J. A., Jayne, S. R., Metzger, E. J.,
514 & Wallcraft, A. J. (2013). Impact of Parameterized Lee Wave Drag on the Energy
515 Budget of an Eddy Global Ocean Model. *Ocean Modelling*, *72*, 119–142. doi:
516 10.1016/j.ocemod.2013.08.006
- 517 Trossman, D. S., Arbic, B. K., Richman, J. G., Garner, S. T., Jayne, S. R., & Wallcraft,
518 A. J. (2016). Impact of Topographic Internal Lee Wave Drag on an Eddy Global
519 Ocean Model. *Ocean Modelling*, *97*, 109–128. doi: 10.1016/j.ocemod.2015.10.013
- 520 Uchida, T., Balwada, D., Abernathey, R., McKinley, G., Smith, S., & Levy, M. (2019). The
521 contribution of submesoscale over mesoscale eddy iron transport in the open southern
522 ocean. *Journal of Advances in Modeling Earth Systems*, *11*(12), 3934–3958. doi:

523 10.1029/2019MS001805

524 Vallis, G. K. (2017). *Atmospheric and oceanic fluid dynamics* (2nd ed.). Cambridge Uni-
525 versity Press.

526 Wunsch, C., & Ferrari, R. (2004). Vertical mixing, energy, and the general circulation of
527 the oceans. *Annu. Rev. Fluid Mech.*, *36*(4), 281 - 314.

528 Yu, X., Ponte, A. L., Lahaye, N., Caspar-Cohen, Z., & Menemenlis, D. (2021). Geostrophy
529 assessment and momentum balance of the global oceans in a tide-and eddy-resolving
530 model. *Journal of Geophysical Research: Oceans*, *126*(10), e2021JC017422. doi:
531 10.1029/2021JC017422

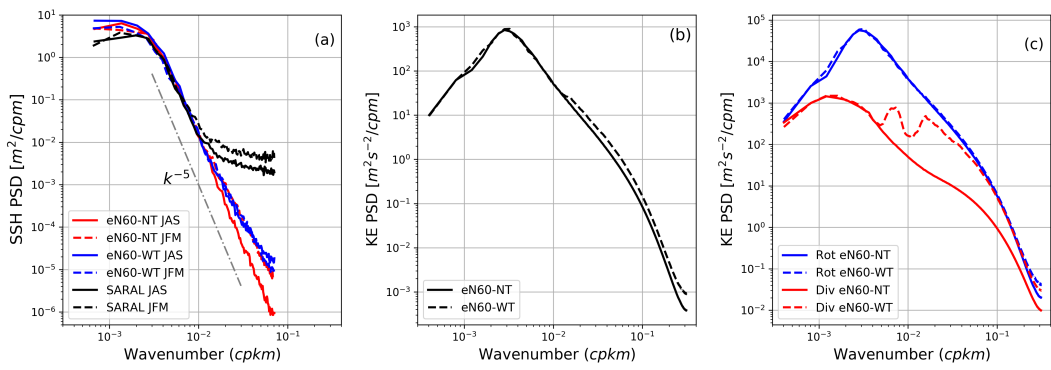


Figure 1. (a) Comparison of SSH wavenumber spectra between eNATL60 and SARAL AltiKa satellite. (b) One year average of surface kinetic energy wavenumber spectral density computed from hourly outputs of eN60-NT (no tides) and eN60-WT (with tides). (c) Helmholtz decomposition of kinetic energy into rotational (ζ) and divergent (δ) spectral components. Thick curves represent the simulation without tides (eN60-NT) and dashed curves represent the simulation with tides (eN60-WT).

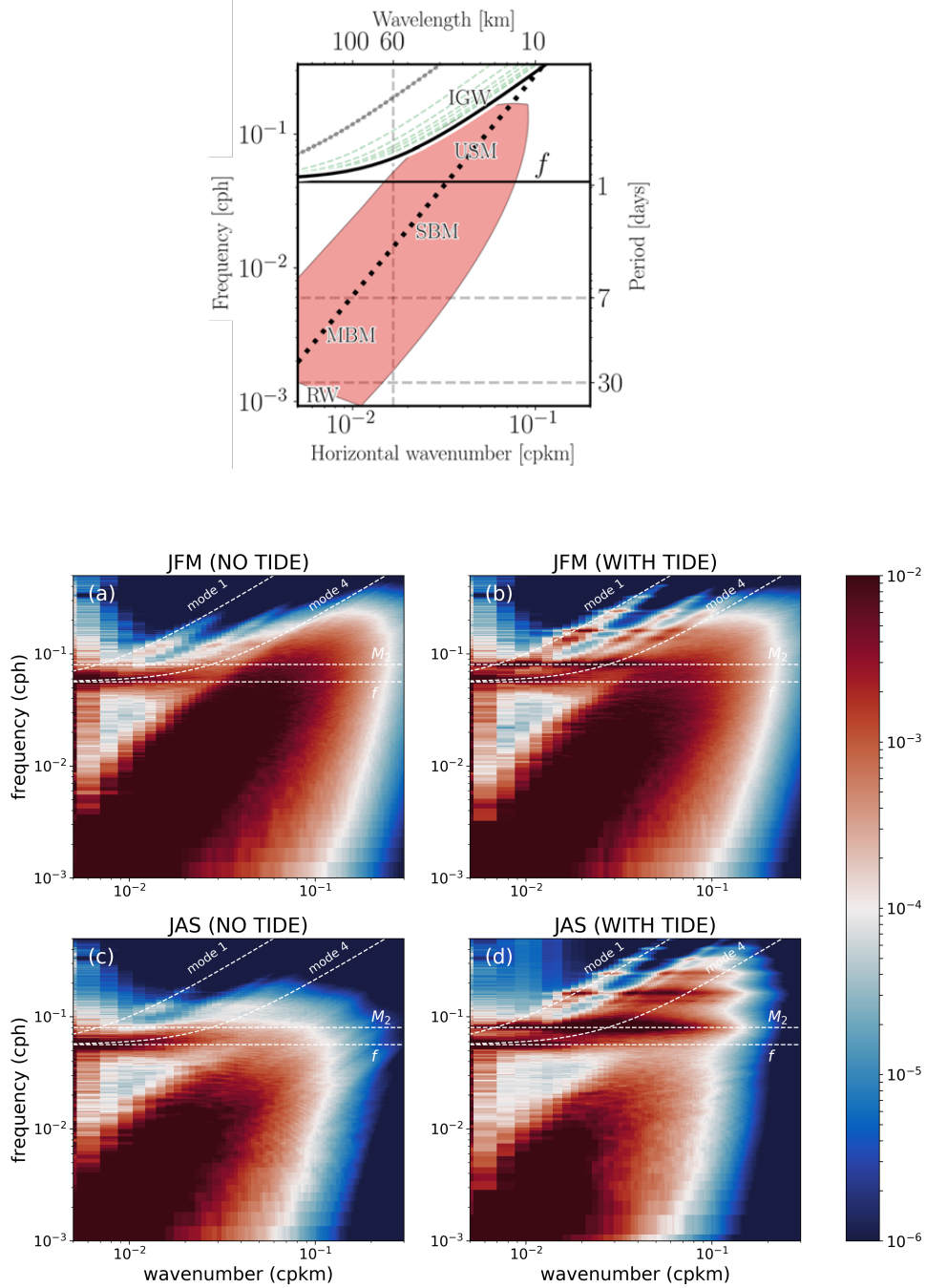


Figure 2. Top panel: A schematic of the observable dynamical regimes with different classes of motions in the ocean. These classes of motions starting with low frequency, small wavenumber motions to high frequency frequency, high wavenumber motions are Rossby waves(RW), mesoscale balanced motions (MBM), submesoscale balanced motions (SBM), unbalanced submesoscale motions (USM) and internal gravity waves (IGW). Bottom four plots: Surface kinetic energy frequency-wavenumber spectra computed from hourly outputs of eN60-NT (no tides) and eN60-WT (with tides) for winter (JFM) and summer (JAS) time.

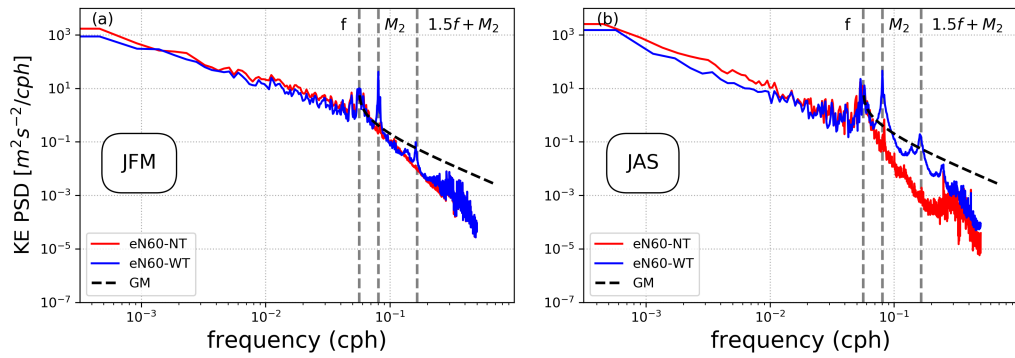


Figure 3. Surface Kinetic energy frequency spectral density, obtained by integrating the ω - K spectra over all wavenumbers for eN60-NT (no tides) and eN60-WT (with tides). The three grey dash lines represent the inertia frequency f , the M_2 tidal frequency, and $1.5f + M_2$. The dashed black line represents the estimate of the Garrett-Munk spectra computed with reference values of total energy of the internal wavefield and stratification set to $E_0 = 6.3e^{-5} m^2 s^{-2}$ and $N_0 = 5.2e^{-3} s^{-1}$, respectively (Garrett & Munk, 1975; Cairns & Williams, 1976; Müller et al., 2015). (a) Winter (JFM) and (b) Summer (JAS).

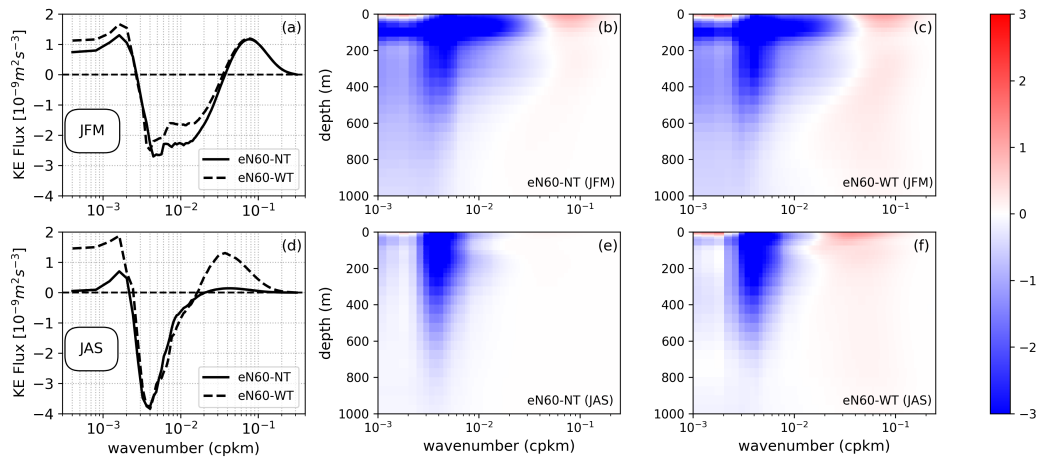


Figure 4. Surface kinetic energy spectral flux computed from hourly outputs of eN60-NT (no tides) and eN60-WT (with tides). Summer : July, August and September. Winter : January, February and March. (b,c,e,f) Winter and summer averages of kinetic energy spectral flux as a function of depth for eN60-NT and eN60-WT.

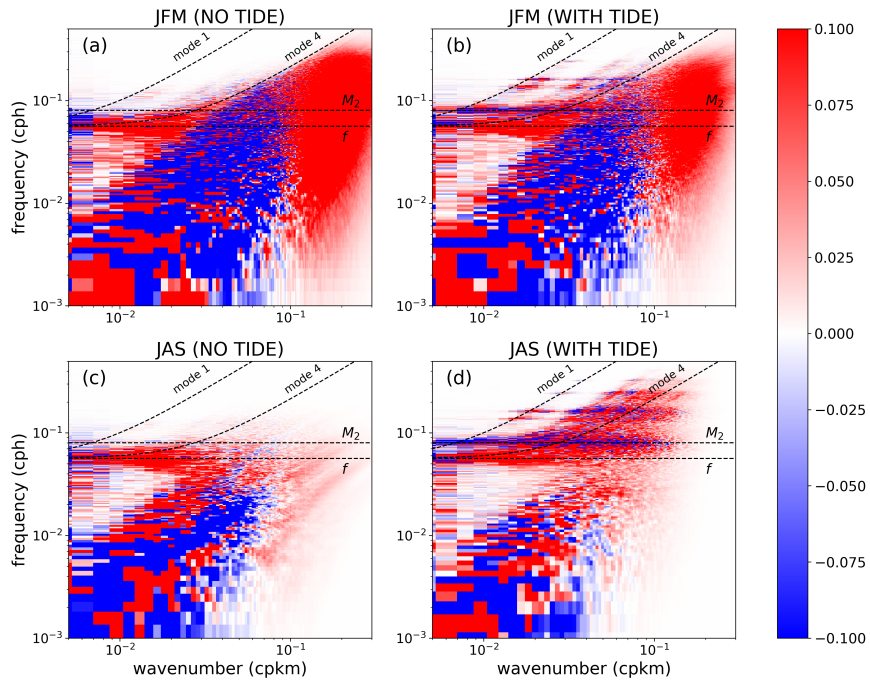


Figure 5. Surface kinetic energy transfer in frequency-wavenumber space computed from hourly outputs of eN60-NT (no tides) and eN60-WT (with tides) for winter (JFM) and summer (JAS) time.